Remote Actuation of Hydrogel Nanocomposites: Heating Analysis, Modeling, and Simulations

Nitin S. Satarkar, Samantha A. Meenach, Kimberly W. Anderson, and J. Zach Hilt
Dept. of Chemical and Materials Engineering, University of Kentucky, Lexington, KY 40506

DOI 10.1002/aic.12309
Published online July 2, 2010 in Wiley Online Library (wileyonlinelibrary.com).

Recently, there has been increasing interest in remote heating of polymer nanocomposites for applications such as actuators, microfluidic valves, drug delivery devices, and hyperthermia treatment of cancer. In this study, magnetic hydrogel nanocomposites of poly(ethylene glycol) (PEG) with varying amounts of iron oxide nanoparticle loadings were synthesized. The nanocomposites were remotely heated using an alternating magnetic field (AMF) at three different AMF amplitudes, and the resultant temperatures were recorded. The rate of the temperature rise and the steady state temperatures were analyzed with a heat transfer model, and a correlation of heat generation per unit mass with the nanoparticle loadings was established for different AMF amplitudes. The temperature rise data of a PEG system with different swelling properties were found to be accurately predicted by the model. Furthermore, the correlations were used to simulate the temperatures of the nanocomposite and the surrounding tissue for potential hyperthermia cancer treatment applications. © 2010 American Institute of Chemical Engineers *AIChE J,* 57: 852–860, 2011

Keywords: biomaterials, biomedical engineering, nanotechnology, heat transfer, composite materials

Introduction

Nanoparticulates, such as iron oxide nanoparticles, gold nanorods and nanoshells, and carbon nanotubes (CNT) can be remotely heated with the application of specific external stimuli, such as radiofrequency fields or near-infrared light.[1] The incorporation of these nanoparticulates into a polymer matrix can result in several interesting properties including improved mechanical, thermal, or electrical behavior,[2] as well as the capability of remote actuation.[3,4] In the last few years, there have been several studies on the remote heating of polymer nanocomposites for a variety of applications, such as actuators,[5–8] microfluidic valves,[9,10] drug delivery devices,[11–15] and for hyperthermia cancer treatment.[16–19]

For example, an alternating magnetic field (AMF) has been shown to selectively induce heating and shape transition in magnetic shape memory polymer nanocomposites.[5,8] In another study, Hawkins et al. demonstrated that addition of iron oxide nanoparticles to a degradable hydrogel matrix can allow heating upon AMF exposure, which was in turn used to manipulate the rates of degradation and drug release.[14] AMF heating has also been explored to trigger the collapse of magnetic nanocomposites of *N*-isopropylacrylamide (NIPAAm), a temperature responsive hydrogel. This phenomenon has been used to demonstrate accelerated drug release, as well as microfluidic valve applications.[10,11,15] In a recent study, Meenach et al. observed favorable cell viability of magnetic NIPAAm nanocomposites with NIH 3T3 murine fibroblasts and also showed heating on the application of

Correspondence concerning this article should be addressed to J. Z. Hilt at hilt@engr.uky.edu.

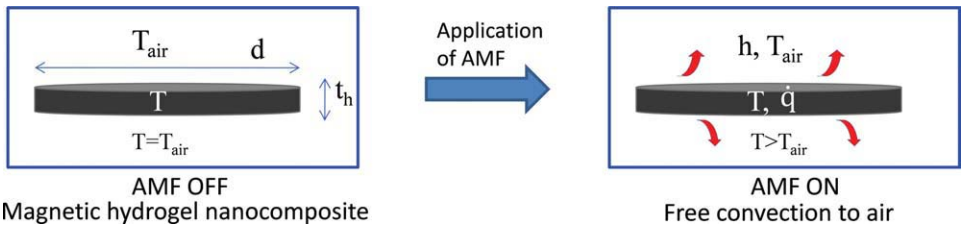

Figure 1. Schematic of a magnetic hydrogel nanocomposite disc subjected to AMF.

Heat generation is by magnetic particles and loss is by convection to surrounding air. [Color figure can be viewed in the online issue, which is available at wileyonlinelibrary.com.]

AMF.[18] In all these studies, heating of the nanocomposites was a key factor, and precise control of the heating would further enhance the system design.

Remote heating of nanoparticles and nanocomposites can also potentially be used for hyperthermia treatment.[16,17] For example, Wang and co-workers developed a Bioglass based degradable magnetic composite and demonstrated selective treatment of lung carcinoma cells by use of an AMF.[19] In another study, Meenach et al. synthesized magnetic poly(ethylene glycol) (PEG) nanocomposites and showed ability to kill glioblastoma cells in vitro with magnetic nanocomposites exposed to AMF.[20] Hyperthermia is the treatment of cancer through the application of heat (41–44°C) and has been under investigation for several decades.[21] Recently, technical advancements in selective heating of superficial and deep-seated tumors has demonstrated significant improvements in the applicability of hyperthermia.[22] A few researchers have looked at modeling magnetic fluid hyperthermia to predict most effective treatment options.[23,24] Additionally, combination of hyperthermia with other treatments, such as radiation therapy and/or chemotherapy can further enhance the treatment success.[25] In addition to those based on magnetic nanoparticles, there has been significant work with polymer nanocomposites containing gold nanoparticles[6,9,12] and CNT.[4,7,13]

Although there have been several interesting demonstrations of remote heating of polymer nanocomposites, modeling of the remote heating still remains unexplored to the best of the author's knowledge. In this article, the analysis of AMF-triggered remote heating of magnetic hydrogel nanocomposites, development of a predictive heat transfer model, and in vivo temperature simulations are reported. PEG hydrogels were selected because of their biocompatibility and their applications as biomaterials, such as in cell encapsulation and controlled therapeutic delivery.[26,27] The analysis of PEG nanocomposite heating at different iron oxide particle loadings and AMF amplitudes was conducted, and a heat transfer model was developed to predict the nanocomposite temperatures. Furthermore, this hydrogel system was aimed at hyperthermia cancer treatment, and hence, COMSOL was used to simulate heating of a nanocomposite disc implanted in tissue.

Development of heat transfer problem

A Model for AMF-induced Heating of Hydrogel Disc

Figure 1 shows a small circular disc of a magnetic hydrogel nanocomposite subjected to AMF and exposed to air. The hydrogel disc in this study was covered in Saran wrap and suspended on top of the solenoid. At any time, the temperature of the nanocomposite disc depends on the rate of heat generation due to magnetic particles and the rate of heat loss to surroundings by convection. The small dimensions of the hydrogel disc coupled with low temperature differentials result in negligible temperature gradients in the disc. Hence, the temperature of the entire disc can be assumed equal to that of the surface. The energy balance on the hydrogel disc is:

$$-hA(T-T_{\text{air}})+\dot{q}m=\frac{d}{dt}(mC_{\text{p,h}}T) \tag{1}$$

where $\dot{q}$ is the rate of heat generation per unit mass of hydrogel and the surface area of the disc is defined by:

$$A=2\pi r^2+2\pi r t_{\text{h}} \tag{2}$$

The experimental setup can be designed to minimize the change in the mass of hydrogels during heating. The heat capacity values for the hydrogel systems under consideration do not change significantly with temperature (see Appendix Table A1). Hence, the analytical solution to Equation (1) using separation of variables and subsequent integration is:

$$T=T_{\text{air}}+\frac{\dot{q}m}{hA}\left\{1-\exp\left[\frac{hA}{mc_{\text{p,h}}}\text{t}\right]\right\} \tag{3}$$

The value of $\dot{q}$ depends on the nanoparticle characteristics and loadings, as well as the AMF properties, such as frequency and amplitude.

At steady state ($t\rightarrow\infty$), Eq. (3) reduces to

$$T_{\text{ss}}=T_{\text{air}}+\frac{\dot{q}m}{hA}\qquad\text{or}\qquad\dot{q}=\frac{hA(T_{\text{ss}}-T_{\text{air}})}{m} \tag{4}$$

Formulation of the in vivo heat transfer problem

The $\dot{q}$ values derived from the analysis of the heat transfer to air can be used for nanocomposite heating in a different environment, if identical AMF amplitudes are achieved. The temperatures of the nanocomposite and its surroundings depend on the heat transfer process and dictate hydrogel performance as an actuator in a microfluidic device, an implant for drug delivery or hyperthermia cancer treatment. As an example, analysis of the nanocomposite disc placed in vivo is discussed here with specific focus on hyperthermia applications.

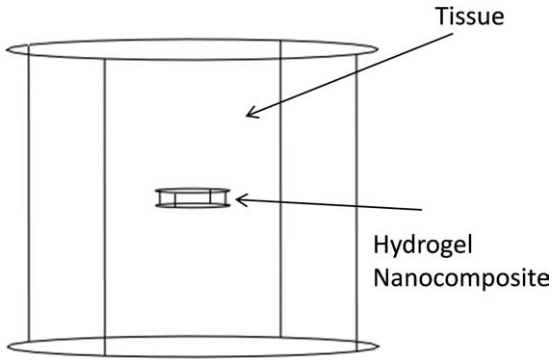

Figure 2. Schematic of hydrogel nanocomposite disc placed at the center of tissue.

To simulate heat transfer between the nanocomposite and surrounding tissue, finite element modeling software COMSOL3.4 was used with the bioheat equation application mode. Here, a hydrogel disc implanted at the center of a cylindrical tissue was considered as the model system (Figure 2). Application of an AMF will result in selective heating of the nanocomposite disc causing the surrounding tissue to heat. Heat transport in the tissue is primarily by conduction with blood perfusion as the other contributing mechanism. Researchers have proposed several models for heat transfer in tissue, and Pennes bioheat equation is the most widely applied and is given below.[28,29]

$$\rho_c C_{p,t} \frac{\partial T}{\partial t} = \nabla \cdot (k_t \nabla T) + \rho_b C_{p,b} w_b (T_b - T) + Q_{met} + Q_{ext} \quad (5)$$

Heat generation from an external source (Q_{ext}) is absent in the tissue region of the model system. Temperature (T) was considered as a continuous variable in the nanocomposite and the tissue regions of the model. The energy balance for the hydrogel nanocomposite region is:

$$\rho_h C_{p,h} \frac{\partial T}{\partial t} = \nabla \cdot (k_h \nabla T) + Q_{ext} \quad (6)$$

The heat generation term (Q_{ext}) is determined by particle loadings and AMF amplitude.

Experimental Analysis

Synthesis of nanocomposites

Poly(ethylene glycol) ($N = 200$) monomethyl ether monomethacrylate (PEG200MMA), tetra(ethylene glycol) dimethacrylate (TEGDMA), and poly(ethylene glycol) ($N = 400$) dimethacrylate (PEG400DMA) were obtained from Polysciences (Warrington, PA). Fe_3O_4 magnetic nanoparticles (20–30 nm diameter, 0.2% PVP-coated) were obtained from Nanostructured and Amorphous Materials (Los Alamos, NM). Initiator ammonium persulfate (APS), accelerator *N*,*N*,*N*′,*N*′-tetramethylethane-1,2-diamine (TEMED), and phosphate buffered saline (PBS) were obtained from Sigma Aldrich (St. Louis, MO). All materials were used as received.

Hydrogels were fabricated via redox polymerization using monomer, crosslinkers, and magnetic particles in varying amounts as indicated in Table 1. PEG200MMA and TEGDMA were used in equimolar ratios for the hydrogel D system. Four different magnetic nanoparticle loadings were added to the hydrogel D system, to look at the effect of particle loadings on the heating in AMF. Hydrogel C2.5, on the other hand, had lower amounts of crosslinker to test the predictive ability of the model. Ethanol was added as the solvent in 1:1 ratio in terms of total weight of the monomer and crosslinker. Various loadings of iron oxide nanoparticles were added in case of hydrogel nanocomposites and the prepolymer solution was bath sonicated for 20 min to obtain even dispersion. APS was added at 2% weight ratio and TEMED was added at 4% weight ratio of total monomer and crosslinker. After combining these materials, the solution was bath sonicated for an additional 2 min, and added to a glass template consisting of two glass plates of size 15 × 15 cm separated with a 0.5 mm Teflon spacer. The gels were kept in the template overnight to ensure complete polymerization and then transferred into deionized water. The water was changed every day for at least 1 week to wash out any unreacted chemicals.

Estimation of nanocomposite properties

After fabrication, the gels were removed from water, cut into circular discs of about 1.4 cm in diameter, and placed in PBS solution. Swelling studies were conducted at 22 and 37°C to obtain the volume swelling ratio (Q) by previously described methods (Appendix equation A1).[18] The volume swelling ratios were also used to estimate hydrogel density.

Heat capacity measurements were performed using differential scanning calorimeter (DSC) (TA Instruments Q200) in the quasi-isothermal modulated DSC mode with data collection for 45 min. Heat capacity values were measured for D0, D5, and C2.5 systems at 22 and 37°C. The hydrogels were equilibrated in PBS at the set temperature for at least 24 h and analyzed at respective temperatures.

Thermal diffusivity values were estimated using flash method[30] with a flash light and controller system (FX 60, Balcar). An infrared camera (SC4000, FLIR Systems) was used to record the surface temperatures (1500 frames per second). The

Table 1. The Compositions of five Different Types of Hydrogels Systems

Abbrev.	Monomer	Mol %	Crosslinker	Mol %	Fe_3O_4 (wt %)
DO	PEG200MMA	50	TEGDMA	50	0
Dl	PEG200MMA	50	TEGDMA	50	1
D2.5	PEG200MMA	50	TEGDMA	50	2.5
D5	PEG200MMA	50	TEGDMA	50	5
C2.5	PEG200MMA	95	PEG400DMA	5	2.5

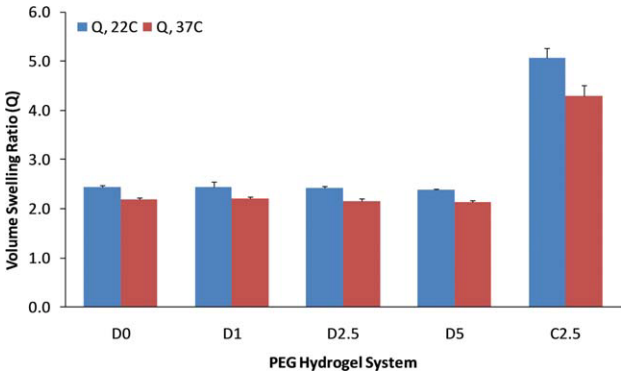

Figure 3. Swelling analysis of the PEG hydrogels at 22 and 37°C $N = 3 \pm$ SD.

[Color figure can be viewed in the online issue, which is available at wileyonlinelibrary.com.]

nanocomposite discs were imbibed in dark brown ink to make them opaque and ensure efficient light absorption.

Heating in an AMF

Hydrogel films were cut into circular discs 8.2 mm in diameter and allowed to equilibrate in PBS overnight at 22°C. Heating was then administered remotely via AMF generated by induction power supply (Taylor Winfield, MMF-3-135/400-2) equipped with a solenoid (1.5 cm diameter, five turns). The hydrogel disc was covered in Saran wrap to limit water evaporation and then placed on top of the solenoid for exposure to the AMF. The hydrogels were exposed to the AMF at about 293 kHz and different AMF amplitudes calculated as 14.8, 19.5, and 25 kA/m. The surface temperature was recorded for first 3 min using infrared camera (AGEMA Thermovision 470). The weight and dimensions of the hydrogel discs were noted before and after heating, and the average of these values were used for calculations.

Statistical analysis

All experiments were performed in triplicates. MYSTAT 12 for Windows (12.02.00) was used for *t*-tests (paired *t*-test with unequal variances) to determine any significance in observed data. A *P*-value of <0.05 was considered statistically significant.

Results and Discussion

Estimation of nanocomposite properties

Figure 3 shows the equilibrium volume swelling ratios (Q) of the hydrogels at 22 and 37°C. Q values decreased slightly at 37°C when compared with 22°C ($P < 0.05$) suggesting a slight temperature responsive nature of PEG hydrogels. This effect implies that the water content of the hydrogel systems will change slightly when exposed to 37°C during in vivo applications. The D systems exhibited less water content than that of the C system, because of a tighter crosslinked network. Thus, the swelling properties of PEG hydrogels can be tailored by changing their composition. For the particle loadings under consideration, the addition of magnetic nanoparticles did not have significant effect ($P > 0.05$) on swelling properties for the D systems.

The DSC measurements showed only a slight effect of temperature on the heat capacity (Appendix Table A1). Additionally, there was negligible effect of particle loadings on $C_{p,h}$ values of PEG D hydrogels. The average of D0 and D5 was used as $C_{p,h}$ for calculations of all the D systems. The thermal diffusivity values were determined by flash analysis method (Appendix equation A2). Thermal conductivity values of the hydrogel nanocomposites were estimated using measured values of density, heat capacity, and thermal diffusivity (Appendix equation A3). Appendix Table A1 summarizes the thermal conductivity values of some of the hydrogel systems.

In the calculation of heat transfer coefficients from the hydrogel surface to surrounding air, the small geometry of the hydrogel disc and low temperature differentials resulted in low values of Rayleigh numbers ($Ra < 100$). Hence, the correlations derived by Chambers et al. for simultaneous convection from top and bottom surfaces of a heated plate were used (Appendix equations A4, A5).[31]

The IR camera recorded only the surface temperatures, whereas the temperature at the center of the disc could be significantly different. Hence, one of the key steps in the heat transfer analysis was to determine if temperature gradients exist in the disc. As $t_h \ll d$, the radial temperature gradients were neglected, and the half thickness of the disc was used as the characteristic length. Using the values of convective heat transfer coefficient, thermal conductivity of hydrogel, and characteristic length, the Biot number (Bi) was calculated to be 4.1×10^{-3} (Appendix equation A6). Thus, lumped parameter analysis (when $Bi < 0.1$) was applied in this case and temperature gradients in the disc were neglected.

Heating in an AMF

The recorded rise in temperatures starting around 25°C is plotted in Figure 4a–c. Heating of magnetic particles when exposed to AMF is attributed to Neel/Brownian relaxations, and hysteresis loss.[32] As expected, increasing the amount of magnetic particles resulted in higher equilibrium temperatures at the same AMF amplitude. Similarly, increasing AMF amplitude led to more heating and higher equilibrium temperatures. There was some resistive heating in case of gels with no magnetic particles.

Comparison of experimental and predicted temperatures

Using Eq. (4) and the steady state temperature values of the D hydrogel nanocomposites (Figure 4), $\dot{q}$ values at different particle loadings and AMF amplitudes were obtained. The $\dot{q}$ values were normalized against volume swelling ratio (Q) of the D systems at 25°C, to allow extension to another temperature or a different hydrogel system. A linear correlation of $\dot{q}$ was obtained with the particle loadings at different AMF amplitudes.

$$\dot{q} = \mathrm{aP} + \mathrm{b} \tag{7}$$

The coefficients a and b at different AMF amplitudes are summarized in Table 2. It is expected that these correlations will be useful in predicting $\dot{q}$ and, in turn, predicting temperatures of the different hydrogel systems.

A MATLAB program was developed to predict the hydrogel temperatures at different time points using Eq. (3). $\dot{q}$

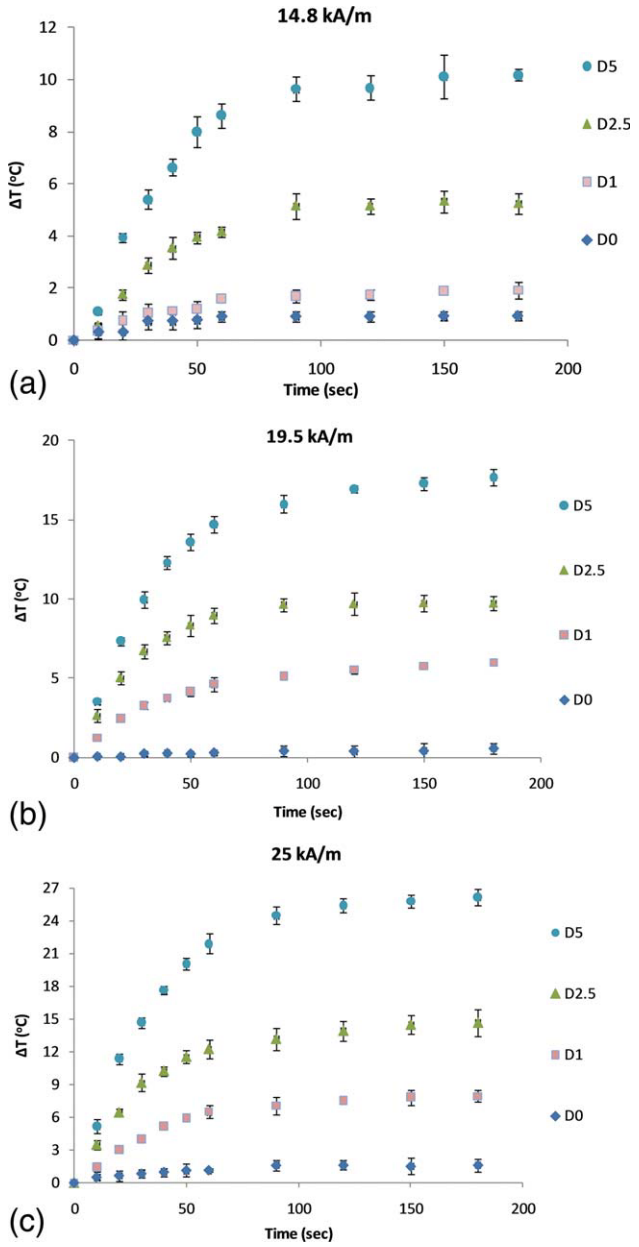

Figure 4. (a–c) Rise in temperature of D nanocomposites for different particle loadings and AMF amplitudes, $N = 3 \pm SD$.

[Color figure can be viewed in the online issue, which is available at wileyonlinelibrary.com.]

correlations from Eq. (7) and coefficients in Table 2 were used along with the measured values of heat capacities and swelling ratios. Heat transfer coefficients were estimated at every time point as the disc temperatures changed. Figure 5a–c shows the comparison of experimental and predicted temperature rise of D hydrogel systems. The plots at different AMF amplitudes demonstrate good fits for the temperature rise. The deviations between the experimental and predicted differentials could be attributed to the loss of water as hydrogel temperatures increased. To simplify the model derivation, hydrogel mass was assumed constant with time. In spite of short heating times and use of Saran wrap, weight

Table 2. Coefficients for $\dot{q}$ Correlations at Different AMF Amplitudes

AMF amplitude (kA/m)	a	b	Regression (R^2) values
14.8	0.2914	0.0473	0.987
19.5	0.5144	0.1684	0.991
25	0.6974	0.3474	0.993

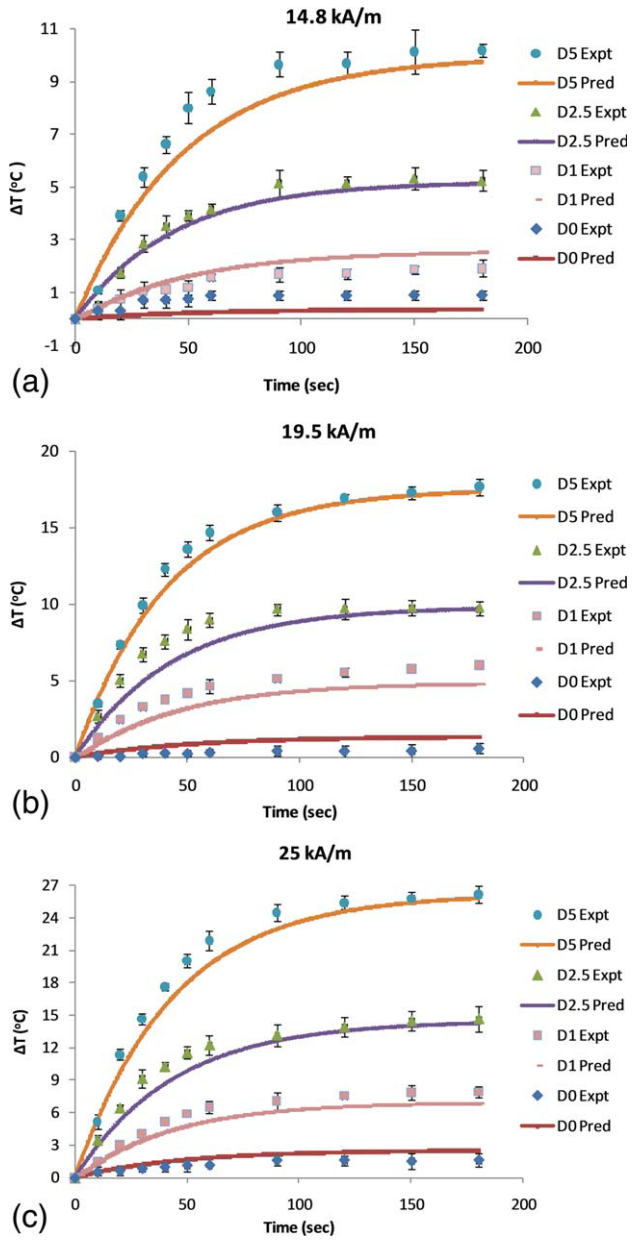

Figure 5. (a–c) Comparison of experimental and predicted rise in temperature of D nanocomposites for different particle loadings and AMF amplitudes, E_{xpt} = Experimental values, P_{red} = Predicted values.

[Color figure can be viewed in the online issue, which is available at wileyonlinelibrary.com.]

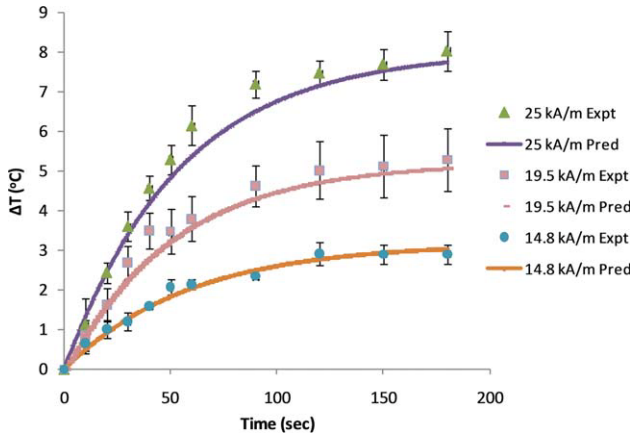

Figure 6. Comparison of experimental and predicted rise in temperature of C2.5 nanocomposites for different AMF amplitudes, E_{xpt} = Experimental values, P_{red} = Predicted values.

[Color figure can be viewed in the online issue, which is available at wileyonlinelibrary.com.]

measurements indicated up to 25% mass loss for the system that was heated the most. Overall, the heat transfer model demonstrated the capability to predict resultant temperatures if the hydrogel properties, AMF amplitude, and heat transfer coefficients are known.

To test the capability of extending the heat transfer model to a different hydrogel system, temperatures of the C2.5 system at different AMF amplitudes were predicted using the model. The C hydrogel system was selected because of significant differences in swelling properties as opposed to the D systems. Higher swelling resulted into lower temperatures due to higher amount of water content. It should be noted that the $\dot{q}$ correlations derived from D hydrogel nanocomposites were used along with the swelling ratios and heat capacity values of C2.5. The predicted temperature differentials are plotted along with observed experimental values in Figure 6. The good agreement between predicted and observed temperature differentials demonstrate that the heat transfer model can be successfully applied to different hydrogel systems. Furthermore, this model can be applied to different mechanisms of remote heating (near-IR, radio frequency) provided that the $\dot{q}$ values can be predicted or determined experimentally.

Prediction of in vivo temperature profiles

To predict the in vivo temperature profiles using COMSOL, initial temperature was set to be 37°C in all domains. Initially, the boundaries were set to insulated, and tissue dimensions were chosen large enough to obtain minimum temperature increase at the boundaries (<2°C). Tissue boundaries were then set to constant temperature of 37°C, and temperatures of the hydrogel nanocomposites as well as surrounding tissue were predicted. After referring to a number of articles,[23,33–35] the following values for constants were chosen for COMSOL simulations: k_t = 0.55 W/m/K, ρ_t = 1000 kg/m^3, C_t = 4186 J/kg/K, ρ_b = 1000 kg/m^3, C_b = 4186 J/kg/K, w_b = 0.0005 s^{-1}, T_b = 310.15 K, Q_{met} = 350 W/m^3. The following properties were estimated experimentally for hydrogel D at 37°C: k_h = 0.464 W/m/K, ρ_h = 1112 kg/m^3, C_h = 2.375 J/kg/K. Heat generation values (Q_{ext}) were determined for a particular particle loading and AMF amplitude based on the $\dot{q}$ correlations.

Figure 7a shows the simulated steady state temperature at the center of hydrogel disc ($x = 0$, $y = 0$, $z = 0$) with radius 4 mm and thickness 0.5 mm placed at the center of tissue with radius 2.5 cm and thickness 4.0 cm. The mesh consisted of 1,64,764 elements. These hydrogel dimensions were identical to the ones used for in vitro experiments. The transient analysis showed that the steady state temperatures are reached within the first 5 min of AMF exposure. As expected, increasing particle loadings and AMF power increased the ability to heat the nanocomposites. The predicted temperature increased to 40°C for the highest particle loadings at the highest AMF amplitude. This implies that the temperatures at the hydrogel edges could be even lower, causing insufficient tissue heating for hyperthermia.

Nanocomposite temperatures in the tissue environment are lower when compared with temperatures in air because of greater conduction rate in tissue than in air. Flow rate of blood in tissue (w_b) also plays an important role in the heat transfer process. Simulations in this study were carried out with blood flowrate value of 0.0005 s^{-1}. The factors that can

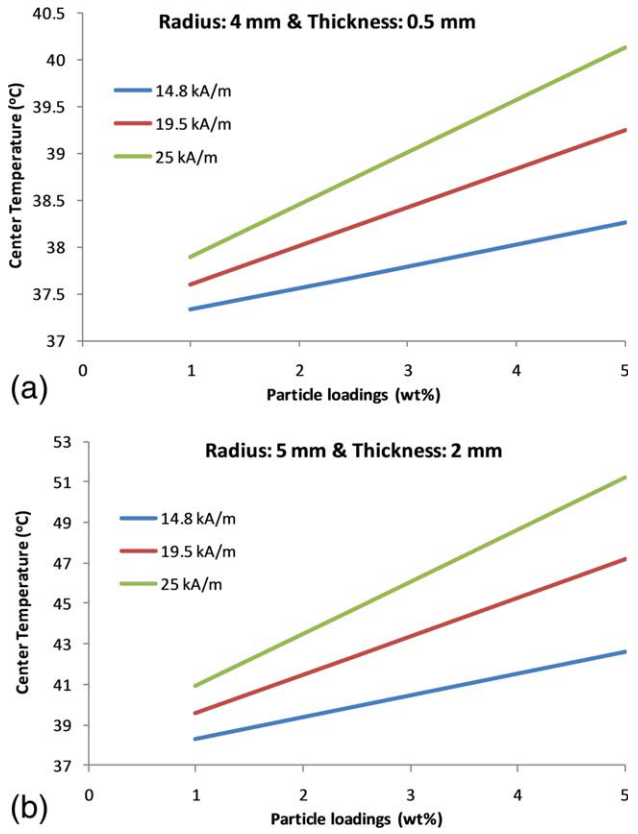

Figure 7. Simulated steady state temperatures at the center of hydrogel disc ($x = 0$, $y = 0$, $z = 0$) placed at the center of tissue with radius 2.5 cm and thickness 4.0 cm.

For (a) Disc radius 4 mm and thickness 0.5 mm, For (b) Disc radius 5 mm and thickness 2 mm. [Color figure can be viewed in the online issue, which is available at wileyonlinelibrary.com.]

influence blood flow include tumor type, size, stage, and site of growth.[21,35] Additionally, perfusion in tumors is quite heterogeneous. Researchers have reported that blood perfusion rates in tumor can vary in the range of 0.0001–0.01 s^{-1}.[36,37] Hence, more information about the site of implant is necessary for accurate prediction of temperatures in specific applications.

Heating can be enhanced by increasing particle loadings, AMF amplitude, or hydrogel dimensions. The derived $\dot{q}$ correlations are for a fixed AMF amplitude and different particle loadings, and hence, they can be extrapolated for higher particle loadings. Furthermore, we have looked at the effect of hydrogel dimensions on resultant temperatures. Temperatures were predicted for a disc of radius 5 mm and thickness 2 mm placed at the center of tissue of radius 2.5 cm and thickness 4 cm. The mesh consisted of 1,29,000 elements. Figure 7b shows that the steady-state temperature at the center of hydrogel reached ~50°C, for 5 wt % particle loadings and 25 kA/m AMF. When hydrogel thickness is increased, the surface area per unit volume decreases resuting in higher temperatures at the center. The simulations can be extended to different types of polymeric systems as potential implants. For example, this temperature rise can be sufficient to cause volume transition in the case of temperature-responsive hydrogels[11] or affect the rate of degradation in the case of degradable polymers.[14]

Figures 8 and 9a, b show simulated steady state temperature profiles of a hydrogel disc (radius 5 mm, thickness 2 mm) with 5 wt % particles and surrounding tissue (radius 2.5 cm and thickness 4 cm) exposed to AMF at a amplitude of 25 kA/m. The temperature profile in an x–z plane along $y = 0$ is plotted in Figure 8. Nanocomposite heating leads to a symmetrical temperature profile in the surrounding tissue. Tissue temperatures are highest at the hydrogel interface and then gradually reduce to that of the body temperature (37°C). Hyperthermia cancer treatment would require heating the tissue in the range of 41–44°C.[25] Figures 9a, b are the temperature profiles in x–y plane (2 cm × 2 cm) at $z = 1$ and $z = 6$ mm, respectively. The model insets highlight z position of the x–y plane. The tissue temperature profile at the hydrogel surface shows that tissue temperatures can reach up to 49°C for these specific conditions [9(a)]. On the other hand, the temperature profile at 5 mm from the hydrogel surface shows that the tissue can heat up to 41°C (9(b)). The tissue temperatures in x–y plane are higher in the region closer to the center of the disc. This implies that the hydrogel can effectively heat a significant amount of tissue to hyperthermia temperatures. The temperature profiles can be effectively modulated by changing hydrogel geometry or use of multiple hydrogel discs. AMF amplitude and particle loadings can also be changed to achieve desired temperatures.

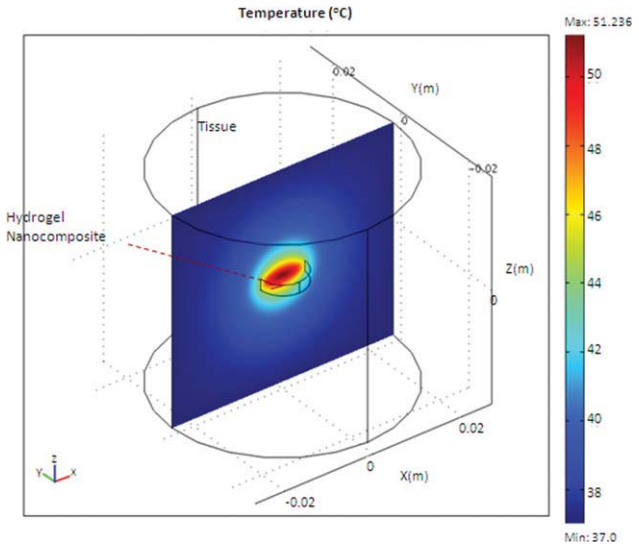

Figure 8. Temperature profile at steady state for hydrogel disc (radius 5 mm, thickness 2 mm, particles 5 wt %, AMF 25 kA/m) and surrounding tissue in x–z plane along $y = 0$.

[Color figure can be viewed in the online issue, which is available at wileyonlinelibrary.com.]

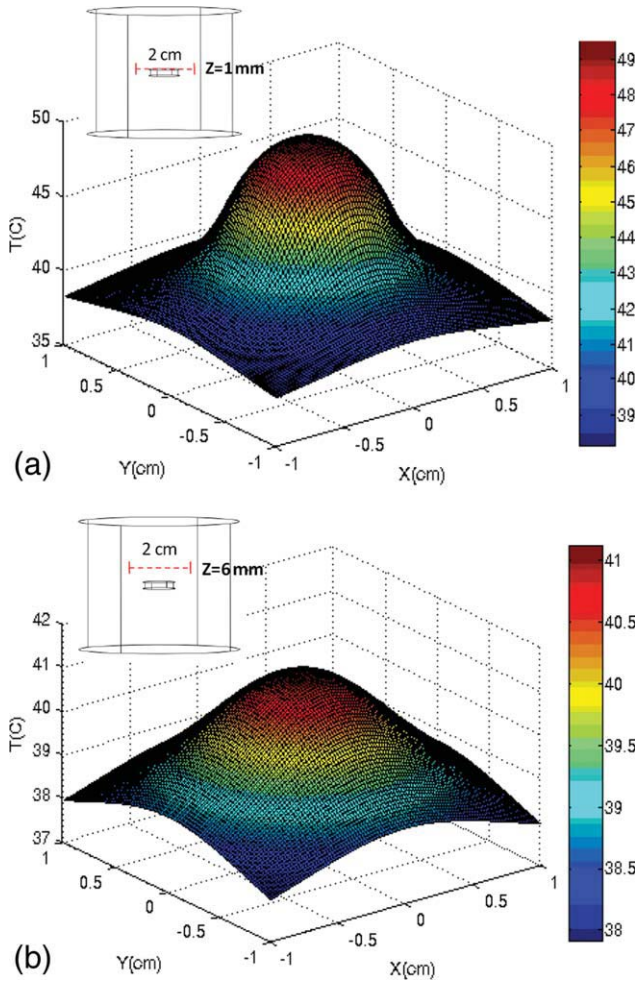

Figure 9. Temperature profile at steady state for hydrogel disc (radius 5 mm, thickness 2 mm, particles 5 wt %, AMF 25 kA/m) and surrounding tissue (a) In x–y plane along $z = 1$ mm, and (b) In x–y plane along $z = 6$ mm.

The model insets highlight z position of the x–y plane. [Color figure can be viewed in the online issue, which is available at wileyonlinelibrary.com.]

Conclusions

Magnetic nanocomposites of PEG hydrogels were synthesized with iron oxide nanoparticle loadings (between 0 and 5 wt %) and remotely heated in an AMF at ~293 kHz. A heat transfer model was proposed for predicting temperature profiles of the hydrogel disc heated with AMF in air environment. Nanocomposite temperatures were collected for AMF amplitudes of 14.8, 19.5, and 25 kA/m, and correlations were established for heat generation ($\dot{q}$) dependence on particle loadings. The temperatures predicted using the model and the $\dot{q}$ correlations were found to be in good agreement with experimentally observed values. The model successfully predicted temperatures of a PEG hydrogel system with different swelling characteristics. For in vivo predictions, temperature profiles of a hydrogel disc and surrounding tissue were simulated using COMSOL, for evaluation as an implant. Although in vivo conditions result in lower hydrogel temperatures, heating profiles can be influenced by hydrogel geometry, particle loadings, and AMF amplitude. Simulations indicated that the nanocomposite heating can raise the surrounding tissue to and above hyperthermia temperatures. It is expected that this study would be helpful for the design of polymer systems heated by various mechanisms and placed in a variety of heat transfer environments.

Acknowledgments

This material is based in part on work supported by the Kentucky Science and Engineering Foundation grant 1169-RDE-009. The authors thank Churn Poh for assistance with thermal conductivity measurements, and Dr. J. Todd Hastings for assistance with COMSOL software.

Notation

A = heat transfer area of the hydrogel disc, m^2
Bi = Biot number
$C_{p,b}$ = heat capacity of blood, J kg^{-1} K^{-1}
$C_{p,h}$ = heat capacity of hydrogel, J kg^{-1} K^{-1}
$C_{p,t}$ = heat capacity of tissue, J kg^{-1} K^{-1}
h = heat transfer coefficient for convection from hydrogel to air, W m^{-2} K^{-1}
k_h = thermal conductivity of hydrogel, W m^{-1} K^{-1}
k_t = thermal conductivity of tissue, W m^{-1} K^{-1}
l = characteristic length
M = mass of the hydrogel disc, kg
Nu = Nusselt number
P = magnetic particle loadings in hydrogel, wt%
Q_{ext} = heat generation from external sources, W m^{-3}
Q_{met} = metabolic heat generation term, W m^{-3}
$\dot{q}$ = rate of heat generation per unit mass of hydrogel, W kg^{-1}
R = radius of the hydrogel disc, m
Ra = Rayleigh number
T = temperature, K
T_{air} = temperature of surrounding air (22°C)
T_{ss} = temperature of the hydrogel disc at steady state, K
$t_{1/2}$ = time required for back surface to reach half of maximum temperature rise, s
t_h = thickness of the hydrogel disc, m
V_d = volume of hydrogel in dry state, m^3
V_s = volume of hydrogel in swollen state, m^3
w_b = blood perfusion rate in tissue, s^{-1}
α = thermal diffusivity of hydrogel, m^2 s^{-1}
ρ_b = density of blood, kg m^{-3}
ρ_h = density of hydrogel, kg m^{-3}
ρ_t = density of tissue, kg m^{-3}

Literature Cited

1. Govorov AO, Richardson HH. Generating heat with metal nanoparticles. *Nanotoday*. 2007;2:30–38.
2. Schexnailder P, Schmidt G. Nanocomposite polymer hydrogels. *Colloid Polym Sci*. 2009;287:1–11.
3. Filipcsei G, Csetneki I, Szilagyi A, Zrinyi M. Magnetic field-responsive smart polymer composites. *Adv Polym Sci*. 2007;206:137–189.
4. Benítez R, Fuentes A, Lozano K. Effects of microwave assisted heating of carbon nanofiber reinforced high density polyethylene. *J Mater Process Tech*. 2007;190:324–331.
5. Mohr R, Kratz K, Weigel T, Lucka-Gabor M, Moneke M, Lendlein A. Initiation of shape-memory effect by inductive heating of magnetic nanoparticles in thermoplastic polymers. *Proc Natl Acad Sci USA*. 2006;103:3540–3545.
6. Zeng X, Jiang H. Tunable liquid microlens actuated by infrared light-responsive hydrogel. *Appl Phys Lett*. 2008;93:151101.
7. Yang L, Setyowati K, Li A, Gong S, Chen J. Reversible infrared actuation of carbon nanotube-liquid crystalline elastomer nanocomposites. *Adv Mater*. 2008;20:2271–2275.
8. Yakacki CM, Satarkar NS, Gall K, Likos R, Hilt JZ. Shape-memory polymer networks with Fe3O4 nanoparticles for remote activation. *J Appl Polym Sci*. 2009;112:3166–3176.
9. Sershen SR, Mensing GA, Ng M, Halas NJ, Beebe DJ, West JL. Independent optical control of microfluidic valves formed from optomechanically responsive nanocomposite hydrogels. *Adv Mater*. 2005;17:1366–1368.
10. Satarkar NS, Zhang W, Eitel RE, Hilt JZ. Magnetic hydrogel nanocomposites as remote controlled microfluidic valves. *Lab Chip*. 2009;9:1773–1779.
11. Satarkar NS, Hilt JZ. Magnetic hydrogel nanocomposites for remote controlled pulsatile drug release. *J Control Relat*. 2008;130:246–251.
12. Bikram M, Gobin AM, Whitmire RE, West JL. Temperature-sensitive hydrogels with SiO2-Au nanoshells for controlled drug delivery. *J Control Relat*. 2007;123:219–227.
13. Miyako E, Nagata H, Hirano K, Hirotsu T. Photodynamic thermoresponsive nanocarbon- polymer gel hybrids. *Small*. 2008;4:1711–1715.
14. Hawkins A, Satarkar N, Hilt J. Nanocomposite degradable hydrogels: demonstration of remote controlled degradation and drug release. *Pharm Res*. 2009;26:667–673.
15. Babincova M, Novotny J, Rosenecker J, Babinec P. Remote radiocontrol of siRNA release from magnetite-hydrogel composite. *Optoelectron Adv Mater*. 2007;1:644–647.
16. Babincová M, Leszczynska D, Sourivong P, Cicmanec P, Babinec P. Superparamagnetic gel as a novel material for electromagnetically induced hyperthermia. *J Magn Magn Mater*. 2001;225:109–112.
17. Ramanujan R, Ang K, Venkatraman S. Magnet-PNIPA hydrogels for bioengineering applications. *J Mater Sci*. 2009;44:1381–1387.
18. Meenach SA, Anderson AA, Suthar M, Anderson KW, Hilt JZ. Biocompatibility analysis of magnetic hydrogel nanocomposites based on poly(N-isopropylacrylamide) and iron oxide. *J Biomed Mater Res A*. 2009;91A:903–909.
19. Wang T-W, Wu H-C, Wang W-R, Lin F-H, Lou P-J, Shieh M-J, Young T-H. The development of magnetic degradable DP- Bioglass for hyperthermia cancer therapy. *J Biomed Mater Res A*. 2007;83A:828–837.
20. Meenach SA, Hilt JZ, Anderson KW. Poly(ethylene glycol)-based magnetic hydrogel nanocomposites for hyperthermia cancer therapy. *Acta Biomater*. 2009. In Press.
21. Hildebrandt B, Wust P, Ahlers O, Dieing A, Sreenivasa G, Kerner T, Felix R, Riess H. The cellular and molecular basis of hyperthermia. *Crit Rev Oncol Hemat*. 2002;43:33–56.
22. Falk MH, Issels RD. Hyperthermia in oncology. *Int J Hyperther*. 2001;17:1–18.
23. Bagaria HG, Johnson DT. Transient solution to the bioheat equation and optimization for magnetic fluid hyperthermia treatment. *Int J Hyperther*. 2005;21:57–75.
24. Candeo A, Dughiero F. Numerical FEM models for the planning of magnetic induction hyperthermia treatments with nanoparticles. *IEEE T Magn*. 2009;45:1658–1661.
25. Horsman MR, Overgaard J. Hyperthermia: a potent enhancer of radiotherapy. *Clin Oncol*. 2007;19:418–426.
26. Schmidt JJ, Rowley J, Kong HJ. Hydrogels used for cell-based drug delivery. *J Biomed Mater Res A*. 2008;87A:1113–1122.

27. Lutz J-F. Polymerization of oligo(ethylene glycol) (meth)acrylates: Toward new generations of smart biocompatible materials. *J Polym Sci A1*. 2008;46:3459–3470.
28. Arkin H, Xu LX, Holmes KR. Recent developments in modeling heat transfer in blood perfused tissues. *IEEE T Bio-med Eng*. 1994; 41:97–107.
29. Pennes HH. Analysis of tissue and arterial blood temperatures in the resting human forearm. *J Appl Physiol*. 1948;1:93–122.
30. Parker WJ, Jenkins RJ, Butler CP, Abbott GL. Flash method of determining thermal diffusivity, heat capacity, and thermal conductivity. *J Appl Phys*. 1961;32:1679–1684.
31. Chambers B, Lee T-YT. A numerical study of local and average natural convection Nusselt numbers for simultaneous convection above and below a uniformly heated horizontal thin plate. *J Heat Transf*. 1997;119:102–108.
32. Vaishnava PP, Tackett R, Dixit A, Sudakar C, Naik R, Lawes G. Magnetic relaxation and dissipative heating in ferrofluids. *J Appl Phys*. 2007;102:063914.
33. Wissler EH. Pennes' 1948 paper revisited. *J Appl Physiol*. 1998;85: 35–41.
34. Hand JW, Lau RW, Lagendijk JJW, Ling J, Burl M, Young IR. Electromagnetic and thermal modeling of SAR and temperature fields in tissue due to an RF decoupling coil. *Magn Reson Med*. 1999;42:183–192.
35. Song CW. Effect of local hyperthermia on blood flow and microenvironment: A review. *Cancer Res*. 1984;44:4721s–4730s.
36. Vaupel P, Kallinowski F, Okunieff P. Blood flow, oxygen and nutrient supply, and metabolic microenvironment of human tumors: A review. *Cancer Res*. 1989;49:6449–6465.
37. Wust P, Hildebrandt B, Sreenivasa G, Rau B, Gellermann J, Riess H, Felix R, Schlag PM. Hyperthermia in combined treatment of cancer. *Lancet Oncol*. 2002;3:487–497.

Appendix

Volume swelling ratio (Q) is given by

$$Q = \frac{V_s}{V_d} \tag{A1}$$

Thermal diffusivity (α) was estimated by flash method[30]

Table A1. Heat Capacity Values of Hydrogel Systems

	Heat capacity (J kg^{-1} K^{-1}) $\times 10^3$		Thermal conductivity (W m^{-1} K^{-1})
System	25°C	37°C	25°C
D0	2.78 ± 0.12	2.34 ± 0.18	0.423 ± 0.03
D5	2.71 ± 0.25	2.41 ± 0.10	0.505 ± 0.12
C2.5	2.86 ± 0.10	3.10 ± 0.27	0.497 ± 0.08

$$\propto = 1.38 \frac{t_h^2}{\pi^2 t_{1/2}} \tag{A2}$$

Thermal diffusivity was in turn used to determine thermal conductivity (k_h)[30]

$$k_h = \propto \rho_h C_{p,h} \tag{A3}$$

Heat transfer coefficients for convection from hydrogel disc to air were determined using following correlations[31]:

For upper surface,

$$\mathrm{Nu} = 0.653\,\mathrm{Ra}^{0.143} \tag{A4}$$

For lower surface,

$$\mathrm{Nu} = 0.979\,\mathrm{Ra}^{0.137} \tag{A5}$$

Biot number (Bi) calculations were performed using following equation:

$$Bi = \frac{h1}{k_h} \tag{A6}$$

Manuscript received Nov. 8, 2009, revision received Feb. 7, 2010, and final revision received May 18, 2010.